MDPI

Article

Cold Plasma Synthesis and Testing of NiO$_X$-Based Thin-Film Catalysts for CO$_2$ Methanation

Martyna Smolarek [1], Hanna Kierzkowska-Pawlak [1], Ryszard Kapica [1], Maciej Fronczak [1], Maciej Sitarz [2], Magdalena Leśniak [2] and Jacek Tyczkowski [1,*]

[1] Department of Molecular Engineering, Faculty of Process and Environmental Engineering, Lodz University of Technology, Wolczanska 213, 90-924 Lodz, Poland; 205615@edu.p.lodz.pl (M.S.); hanna.kierzkowska-pawlak@p.lodz.pl (H.K.-P.); ryszard.kapica@p.lodz.pl (R.K.); maciej.fronczak@p.lodz.pl (M.F.)

[2] Department of Silicates and Macromolecular Compounds, Faculty of Materials Science and Ceramics, AGH University of Science and Technology, 30-059 Kraków, Poland; msitarz@agh.edu.pl (M.S.); mlesniak@agh.edu.pl (M.L.)

* Correspondence: jacek.tyczkowski@p.lodz.pl

Abstract: An essential problem in managing CO$_2$ and transforming it into methane as a useful fuel is the quest for adequately efficient and cheap catalysts. Another condition is imposed by the new designs of structured reactors, which require catalysts in the form of the thinnest possible films. The aim of this work was to produce Ni-based thin-film catalysts by the cold plasma deposition method (PECVD) from a volatile metal complex (Ni(CO)$_4$) and to study their structure and catalytic properties in the CO$_2$ methanation process. We tested three basic types of films: as-deposited, calcined in Ar, and calcined in air. The nanostructure and molecular structure of the films were investigated by electron microscopy (SEM), X-ray diffraction (XRD), and X-ray photoelectron spectroscopy (XPS). The catalytic activity was evaluated in the methanation process (CO$_2$ + H$_2$), which was performed in a tubular reactor operating in the temperature range of 300–400 °C. The films calcined in air showed the highest activity in this process but behaved unstably. However, their regeneration by recalcination in air restored the initial catalytic activity. An important conclusion emerged from the obtained results, namely that the active phase in the tested films is Ni^{3+} (most likely in the form of Ni$_2$O$_3$), contrary to the common opinion that this phase is metallic Ni^0. In our case, Ni^0 quenches the catalytic activity.

Keywords: Ni-based catalysts; thin-film nanocatalysts; cold plasma deposition (PECVD); CO$_2$ methanation; nickel oxides

1. Introduction

The technology for the production of thin films using the cold plasma deposition method (PECVD) has opened the possibility of obtaining a completely new generation of catalytic materials with wide prospects for their application in various chemical and photo-electrochemical processes [1–3]. The main advantage of this type of catalytic materials is their thin-film nature (thickness from several tens of nm to several μm) and the possibility of deposition on supports of virtually any shape without changing their original geometry, which is extremely useful in the construction of structured packings for chemical reactors [4]. Not without significance is also the relatively easy and precise control of the molecular structure and nanostructure of such films, which is realized in a wide range by selecting the appropriate plasma precursors and the conditions of the production process [5,6].

In recent years, there has been enormous interest in using CO$_2$ to produce a variety of useful products, especially methane as a very valuable fuel. This is related to both the widespread belief in the negative role of CO$_2$ in global warming and the treatment of CO$_2$ as a wonderful source of "pure" carbon, opening the way to various useful syntheses [7–9].

Among the many catalysts tested in the CO_2 methanation process, nickel-based catalysts belong to the most active in this process and are simultaneously relatively cheap, so it is no wonder that these catalysts receive a lot of attention [10–13]. However, despite intensive research, the optimal Ni-based catalyst for the CO_2 methanation process has not yet been indicated. On the other hand, a wide base of results has already been gathered showing large differences in the process performance and the catalyst stability depending on the type of support material, preparation methods, and the additives [14–19], supplementing the base constantly with new, more and more sophisticated systems, such as decorating carbon nanotubes doped with nitrogen with nickel nanoparticles [20] or nickel loading on graphene nanosheets [21].

Another unresolved problem is the determination of the nature of the active centers in Ni-based catalysts, which participate in the CO_2 methanation process [22,23]. Initially, it was thought, which is still often claimed today, that the only active phase is metallic nickel (Ni^0) [24–26]. However, subsequent studies showed the complex structure of such catalysts [27], in which NiO (Ni^{2+}) began to be assigned a special role [28–30]. Some attention should also be paid to Ni_2O_3 (Ni^{3+}), which appears in Ni-based catalysts, and its activity has already been suggested in the CO_2 methanation process [31,32].

Many different methods are used to prepare Ni-based catalysts, such as impregnation, deposition-precipitation, co-precipitation, sol-gel, ion exchange, flame synthesis, or the recently described new spray-drying method [30,33]. In some cases, the plasma technique was also involved in the preparation of nickel catalysts for methanation. It focused mainly on the dielectric barrier discharge (DBD) method used both in the process of initial catalyst formation and its final activation. It was found that such a procedure improved the catalytic properties and provided better anti-carbon deposit performance compared to the catalyst made only by thermal treatment [34–38]. It should be noted, however, that this is only a plasma treatment of "classically" produced catalysts. Despite the already successful use of Co-based plasma-deposited thin-film catalysts in the CO_2 methanation process [3–5], to our knowledge, Ni-based plasma-deposited catalytic films have not been tested so far in this process.

In this study, an attempt was made to obtain Ni-based thin-film catalysts from a volatile metal complex ($Ni(CO)_4$) by the PECVD method, and preliminary investigations of their structure and catalytic properties in the CO_2 methanation process were carried out.

2. Results and Discussion

The catalytic films were deposited by the PECVD method from $Ni(CO)_4$ on a support made of kanthal steel covered with a layer of Al_2O_3 by high-temperature calcination. Three types of films were then investigated: as-deposited films (ad-NiO_X), thermally treated at 400 °C after deposition in an argon atmosphere (Ar-NiO_X), and treated in the same way in an air atmosphere (air-NiO_X). Scanning electron microscopy (SEM) observations showed, in each of these cases, uniform coverage of the support surface by the deposited films, revealing at the same time their globular morphology (Figure 1a–c). The grain size distribution analysis indicates no significant differences in surface morphology between these three types of films. Only a slightly larger average grain size (by approximately 14%) was observed for the Ar-NiO_X film compared to the ad-NiO_X and air-NiO_X films (Figure 1d–f). It should be added that after the methanation process (400 °C, 37 h), the surface morphology of the catalytic films practically does not change. As an example, SEM images for the air-NiO_X film before and after this process are shown in Figure 2.

Catalytic testing of the methanation process was carried out in a tubular reactor (described in Ref. [39]) using a stoichiometric reaction mixture of CO_2 and H_2 (1:4). In this process, in addition to methane, a certain amount of by-product was also identified, which, in this case, was carbon monoxide. Figure 3a shows the dependencies of selectivity to CH_4 and CO as a function of the process temperature for the three tested types of catalytic films. In turn, Figure 3b presents the CO_2 conversion and CH_4 yield depending on the tempera-

ture at which the methanation process was carried out. The values shown in Figure 3 were determined for the initial stage of the methanation process at a given temperature.
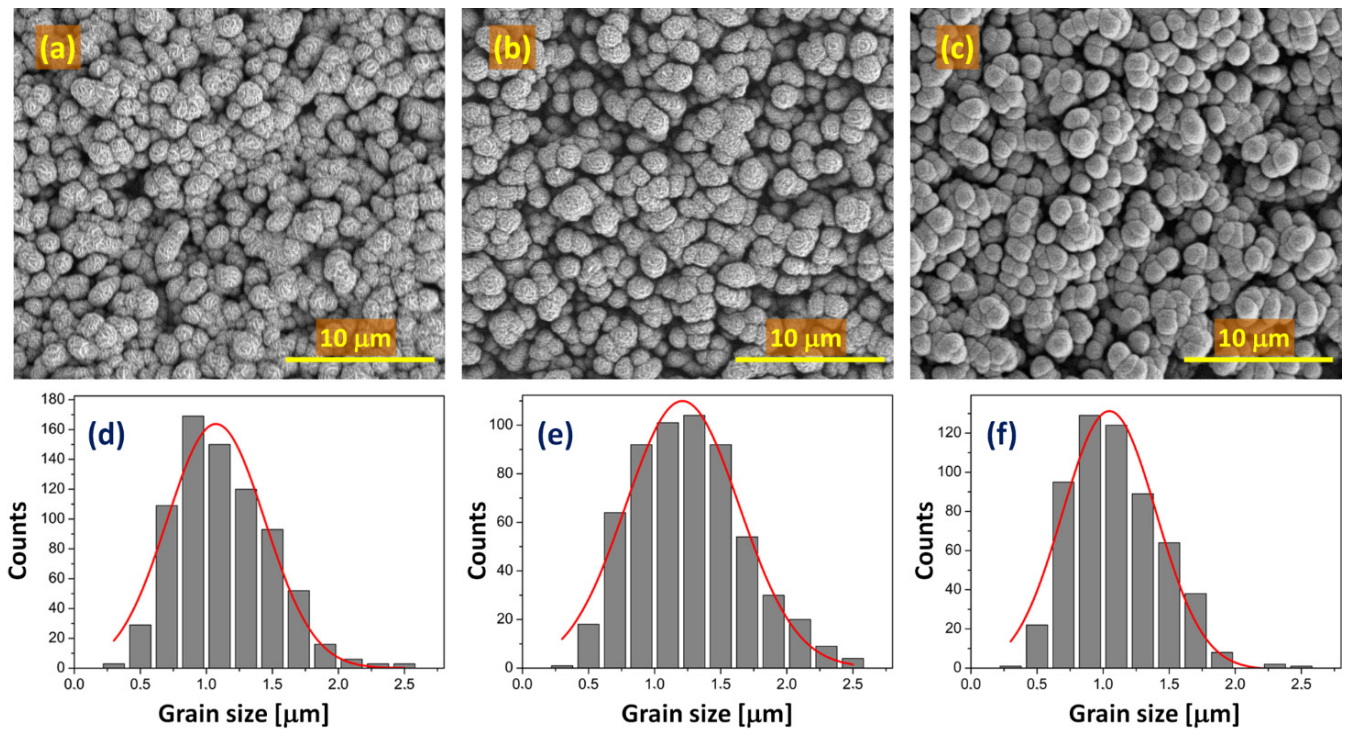

Figure 1. SEM images of the three types of plasma-deposited Ni-based films and the corresponding grain size distributions: (**a**,**d**) ad-NiO_X; (**b**,**e**) Ar-NiO_X; (**c**,**f**) air-NiO_X.
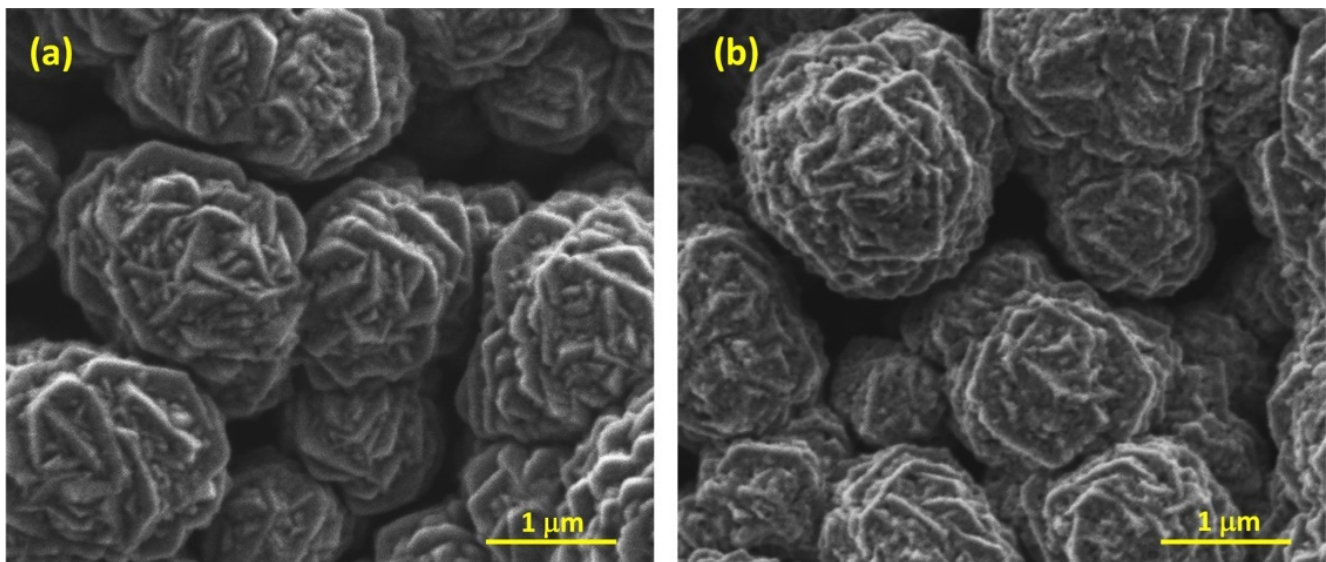
Figure 2. SEM images of the air-NiO_X film: (**a**) Before and (**b**) After 37 h of the methanation process (spent catalyst).

When analyzing the catalytic properties, apart from the determined instantaneous values of conversion and selectivity, the stability of these parameters is of particular importance. The results of CO_2 conversion and CH_4 selectivity measurements as a function of time for the tested types of catalytic films and for different temperatures of the methanation process are shown in Figure 4a.
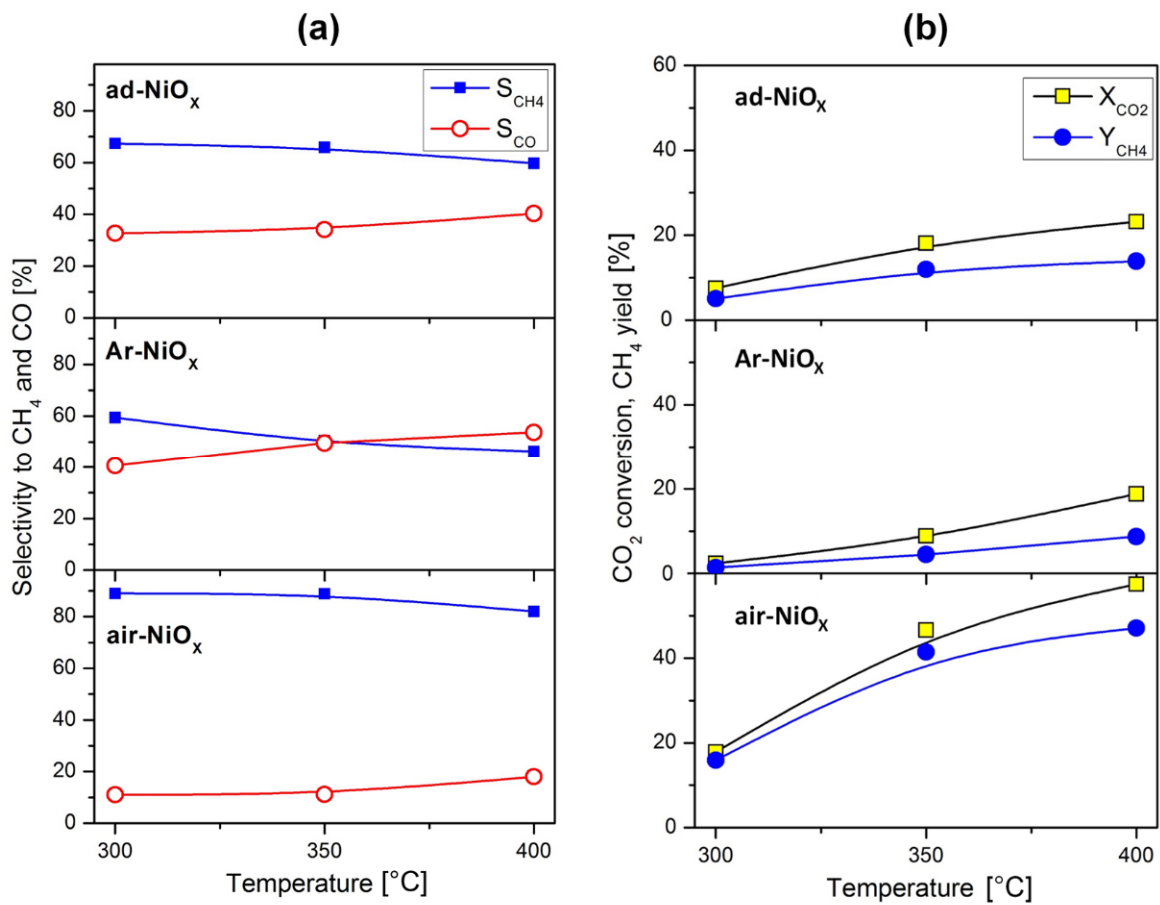
Figure 3. Catalytic activity of plasma-deposited Ni-based films in the initial stage of the methanation process: (**a**) Selectivity to CH_4 and CO; (**b**) CO_2 conversion and CH_4 yield.
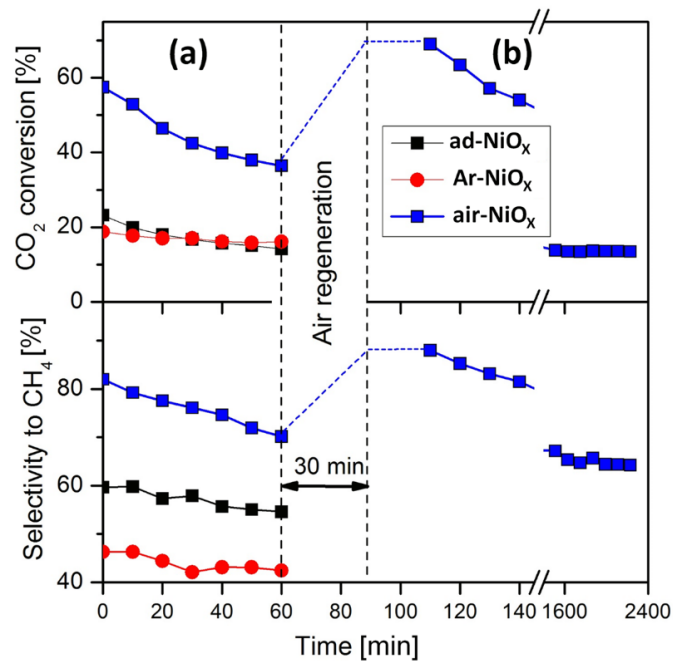

Figure 4. CO_2 conversion and selectivity to CH_4 (at 400 °C) as a function of time-on-stream for the three types of plasma-deposited Ni-based films: (**a**) First run (fresh catalysts); (**b**) the next run after regeneration.

As can be seen, the air-NiO_X films provide the best selectivity and yield of methane production. On the other hand, however, these films are characterized by relatively poor catalytic stability. At the temperature of 400 °C in the first hour of the methanation process, the CH_4 yield drops from 47 to 25% (calculated from Figure 4a). As it turned out, the air-NiO_X films can be easily regenerated. Interruption of the methanation process and thermal re-treating the catalytic film in air for 30 min restores its initial CH_4 yield, which in turn decreases again with the duration of methanation (Figure 4b). Thus, the regeneration process is reversible, and in that case, much easier than in the case of permanent changes in the structure, it will be possible to try to inhibit the deactivation process through an appropriate molecular design, for example, by doping or creating a proper nanocomposite structure, which will allow for obtaining a stable and active catalyst based on the tested films. The PECVD technique makes it possible to easily implement such ideas using the co-deposition technique (for example, see Ref. [39]).

To better explore the nature of the plasma deposited Ni-based films and, consequently, to better understand their catalytic properties, studies of the nanostructure (XRD) and the surface molecular structure (XPS) of these films were carried out. XRD patterns of the ad-NiO_X, Ar-NiO_X, and air-NiO_X are shown in Figure 5. As the XRD analysis shows, the ad-NiO_X film undoubtedly contains metallic nickel nanoparticles with a hexagonal structure (hcp), as evidenced by reflections at 38.8° (010), 41.9° (002), 58.5° (012), 70.3° (110), and 78.2° (103) [40,41]. In addition, there is one more distinct diffraction peak (at 44.3°) in this spectrum, the interpretation of which is more difficult. It can also be assigned to the Ni hcp structure as the reflection corresponding to the (011) plane, or as the reflection (111) for the Ni fcc structure. However, the latter case is unlikely because no other diffraction peaks for the Ni fcc structure can be seen here [40,41]. Meanwhile, at the 44.2° position, a diffraction peak for NiO is also predicted [42]. The presence of NiO in the film is confirmed by weak reflection at 37.3° [43]. In turn, the weak diffraction peak at 32.8° can be attributed to the Ni_2O_3 structure [44–46].

After thermal treatment at 400 °C, in both the argon and air atmosphere, a drastic change in the structure of metallic nickel is observed. Its full phase transition from hcp to fcc takes place, as evidenced by the complete disappearance of the hcp diffraction peaks visible for the ad-NiO_X sample and the appearance of typical reflections for the fcc structure at 44.6° (111), 51.9° (200) and 76.4° (220) for the Ar-NiO_X and air-NiO_X samples. This result is understandable given the fact that the Ni fcc is the more thermodynamically stable nickel crystal structure, and hence temperature induces the hcp to fcc transformation [40]. Moreover, the diffraction patterns for these films, similarly as in the case of the ad-NiO_X film, indicate the presence of NiO and Ni_2O_3 in their composition. This is particularly evident for the air-NiO_X film, where the NiO structure is shown by reflections at 37.5° and 63.0°, as well as at 44.3°, of which the peak probably overlaps with that of Ni fcc (111). The presence of Ni_2O_3 is evidenced by the reflection at 32.8° and presumably also by the diffraction peak at 43.3°, which could optionally be associated with this oxide [46].

The XRD analysis only provides information about the averaged structure of the entire sample, whereas catalytic processes take place on the sample surface and therefore its molecular structure is primarily of particular importance. The performed XPS investigations allowed for a more precise determination of this structure and an attempt to connect it with the catalytic process of methanation. XPS wide-scan spectra for ad-NiO_X, Ar-NiO_X, and air-NiO_X films before (fresh) and after the catalytic process (spent) revealed that in all these cases the films are composed of three elements: nickel, oxygen, and carbon (hydrogen is not detected). The determined elemental atomic composition of these samples is presented in Table 1.
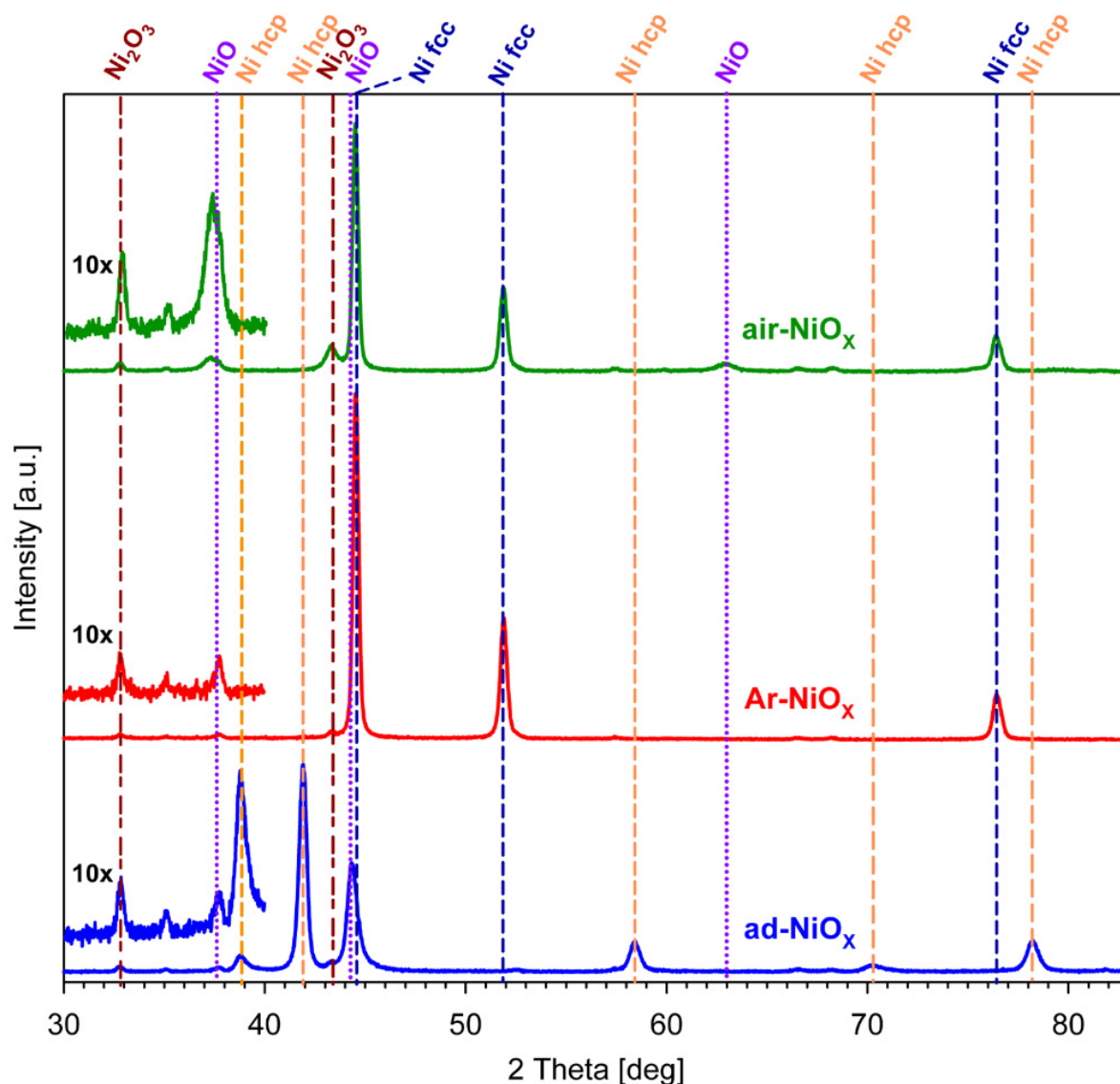
Figure 5. XRD patterns for the three types of fresh plasma-deposited Ni-based films: as-deposited (ad-NiO$_X$), calcined in argon (Ar-NiO$_X$), and calcined in air (air-NiO$_X$).

Table 1. Elemental atomic composition of the fresh and spent plasma-deposited Ni-based films.

Catalyst →	ad-NiO$_X$ Fresh	ad-NiO$_X$ Spent	Ar-NiO$_X$ Fresh	Ar-NiO$_X$ Spent	air-NiO$_X$ Fresh	air-NiO$_X$ Spent
Element ↓	Content [at %]					
Ni	30.6	33.6	1.2	1.5	31.3	33.5
O	30.2	27.6	5.2	4.2	39.6	41.7
C	39.2	38.8	93.6	94.3	29.1	24.8

Comparing the composition of the fresh films, it is easy to notice the drastic difference between Ar-NiO$_X$ film and the other two films, where the surface of the former is composed mainly of carbon and a very small amount of nickel and oxygen. Obviously, the thermal treatment with argon could not cause the removal of nickel. Thus, carbon most likely diffuses to the surface of the film from its bulk. In this way, it covers a significant part of catalytically active nickel structures, which is reflected in low CO$_2$ conversion (Figure 3b). The carbon coating also increases the size of the globules observed by SEM, as shown by the

analysis of the surface morphology (Figure 1d–f). In turn, when comparing the ad-NiO$_X$ and air-NiO$_X$ films, we see practically the same nickel content, while the air-NiO$_X$ film has a clearly lower carbon content and a higher oxygen content, which is due to the "burning" of carbon and the chemical bonding of oxygen in the film during thermal treatment in air. The methanation process carried out on the tested films does not cause significant changes in their surface composition (spent samples). An important conclusion, however, is finding that there is no increase in the carbon content on the surface of the catalytic films during this process, which proves that no carbon deposit is formed there. This is a promising result for Ni-based thin-film catalysts. In general, carbon deposit is a significant problem in the case of the methanation process using Ni-based catalysts [27,47].

To look deeper into the molecular structure of the studied catalytic films, the region corresponding to Ni 2p in the XPS spectra was analyzed in detail. The core-level spectrum of Ni 2p was numerically deconvoluted and the obtained bands were assigned to appropriate species, in accordance with the literature [48–52]. This spectrum is a spin-orbit split into a doublet, Ni 2p$_{3/2}$ and Ni 2p$_{1/2}$ bands, which reveal the same chemical oxidation states of nickel. Therefore, only the more intense Ni 2p$_{3/2}$ band was analyzed. Figure 6 shows the spectra of this band after deconvolution for all three investigated types of fresh films. The figure also shows an example of the Ni 2p$_{3/2}$ band for the air-NiO$_X$ sample after the methanation process (spent catalyst).
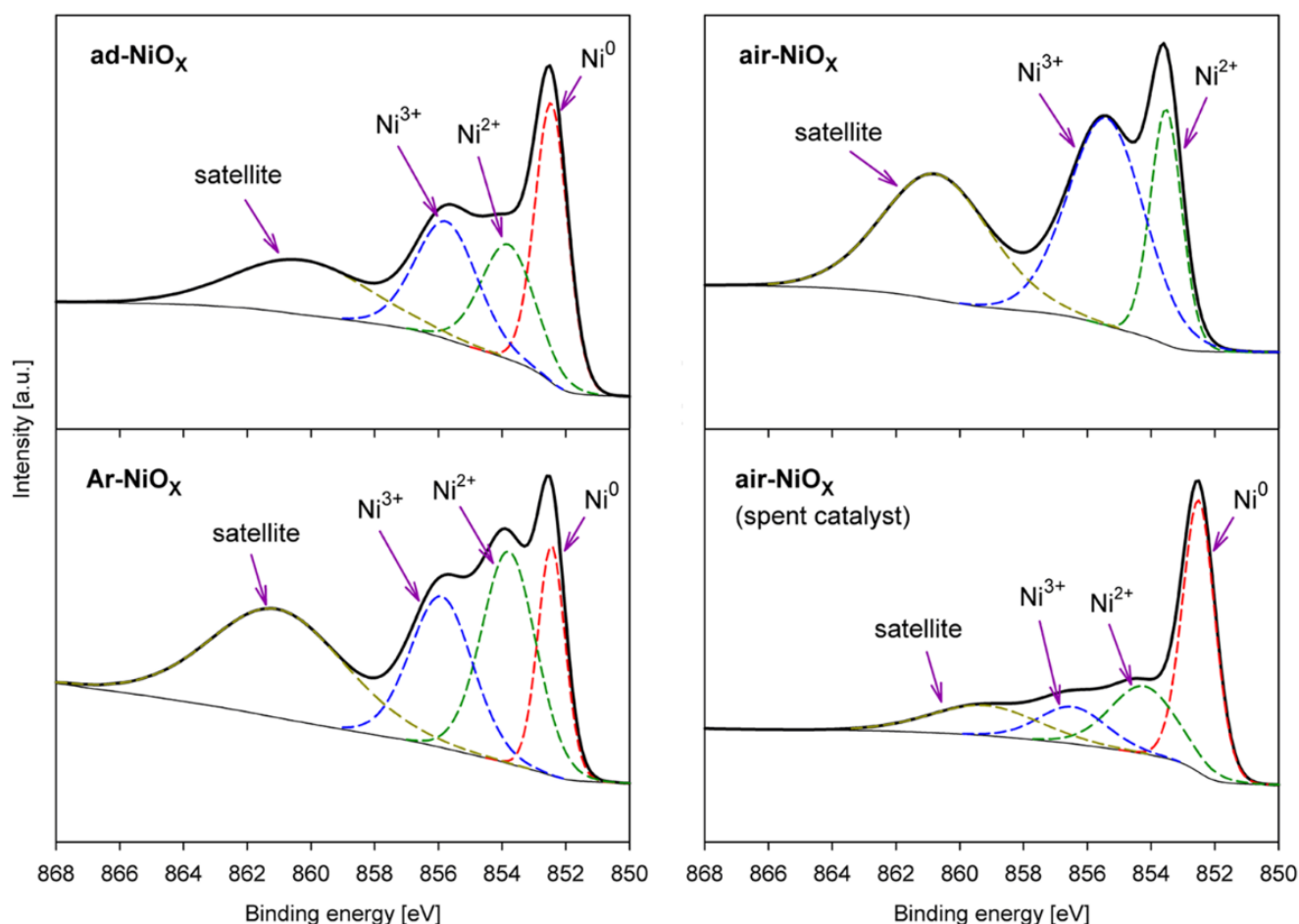
Figure 6. XPS Ni 2p$_{3/2}$ spectra for all tested types of fresh plasma-deposited Ni-based films (ad-NiO$_X$, Ar-NiO$_X$, and air-NiO$_X$), as well as for the air-NiO$_X$ film after 37 h of the methanation process (spent catalyst).

The Ni 2p$_{1/2}$ band can be fitted with four sub-bands assigned to (1) metallic Ni (Ni^0) at 852.4 eV, (2) Ni^{2+} oxidation state at 853.5–854.2 eV, which is related to NiO, (3) Ni^{3+} oxidation state at 855.4–856.5 eV, which is related to Ni$_2$O$_3$, and (4) a broad satellite peak at

approximately 860–861 eV. To determine the quantitative relationship between different Ni oxidation forms, their contents are summarized in Table 2. The surprising conclusion from these results is that the surface of the air-NiO_X film, which shows the best catalytic properties (Figure 3a,b), does not contain the metallic form of nickel (Ni^0), and only the oxidized forms (Ni^{2+} and Ni^{3+}) are present. It should be noted here, taking into account the XRD results (Figure 5), that the XPS analysis examines only a very thin surface layer (about 10 nm). Thus, Ni^0 may be present in the bulk of the air-NiO_X film (as shown by XRD analysis), although this form is not on the surface. During the methanation process, the Ni^{2+} and Ni^{3+} forms are clearly reduced to Ni^0, with a simultaneous significant decrease in CO_2 conversion. A similar effect of the increase in Ni^0 content at the expense of oxidized forms is also observed for the other two types of films (ad-NiO_X and Ar-NiO_X), which is accompanied by a decrease in CO_2 conversion (Figure 4a).

Table 2. Nickel and carbon speciation composition of the fresh and spent plasma-deposited Ni-based films.

Catalyst →	ad-NiO_X Fresh	ad-NiO_X Spent	Ar-NiO_X Fresh	Ar-NiO_X Spent	air-NiO_X Fresh	air-NiO_X Spent
Ni speciation ↓			Content [at %]			
Ni^0	40.5	69.0	32.1	63.6	0.00	55.7
Ni^{2+}	29.3	20.4	44.0	36.4	32.9	28.1
Ni^{3+}	30.2	10.6	23.9	0.00	67.1	16.2
C speciation ↓			Content [at %]			
C−C/C−H (sp³)	10.8	9.1	13.4	13.1	7.7	13.8
C=C (sp²)	71.2	78.5	72.4	83.4	86.4	69.9
C−O/C=O	18.0	12.4	14.2	3.5	5.9	16.3

The very similar nickel content in the surface of ad-NiO_X and air-NiO_X films, for both fresh and spent samples (Table 1), allows us to try to link the content of nickel forms in these films with the performance of the CO_2 conversion process. The content of Ni^0 in the fresh ad-NiO_X film is high and is about 40.5 at %, while the air-NiO_X film, as already mentioned above, completely does not contain this form. In turn, the Ni^{2+} content is similar, whereas the Ni^{3+} content in the air-NiO_X film is more than twice as high as in the ad-Ni film and amounts to as much as 67.1 at %. Accordingly, it can be concluded that over 3 times higher CH_4 yield on the air-NiO_X catalytic film than on the ad-NiO_X film (Figure 3b) results from the presence of nickel in the third oxidation state (Ni^{3+}), and most likely in the Ni_2O_3 structure. In the spent samples, the content of Ni^0 increased significantly, while the content of Ni^{3+} decreased drastically. However, the concentration of Ni^{2+} decreased only slightly. These changes in the Ni-based structure are clearly associated with a decrease in the efficiency of the methanation process and evidently indicate an association of Ni_2O_3 with the process. If we regenerate the spent catalyst film, as it was done with the air-NiO_X film (Figure 4b), the original molecular structure of the film is practically reconstructed, which is accompanied by a return to the initial catalytic activity in the methanation process. These interesting findings require further study to determine the role of Ni^{3+} in the catalytic mechanism, which can be quite complex, for example, through the interaction of Ni^{3+} with Ni^{2+} [42], as well as to search for the possibility of ensuring the stability of the catalyst, for example by adding appropriate promoters [53,54].

When analyzing the influence of the molecular structure of the investigated catalytic films on the CO_2 methanation process, one should also take into account carbon structures, which often play a very important role in catalytic processes [55,56]. In our case, carbon is introduced into the structure of the films during the plasma deposition process, and its source is the $Ni(CO)_4$ precursor. Figure 7 presents the XPS spectra of the deconvoluted C 1s

band for all three investigated types of fresh films and for the air-NiO$_X$ sample after the methanation process (spent catalyst). Generally, there are five basic sub-bands in the C 1s band, which we have assigned, based on the literature [5,57,58], to (1) sp^2 carbon (C=C) at 284.4 eV, (2) sp^3 carbon (C−C, C−H) at 285.1–285.9 eV, (3) carbon single-bonded to oxygen (C−O) at 286.3–287.2 eV, (4) carbon doubly bonded to oxygen (C=O) at 287.9–288.8 eV, and (5) a broad sub-band at above 290 eV, related to the strongly oxidated carbon and recorded only in the Ar-NiO$_X$ sample with a very high carbon content (Table 1). The concentrations of the various forms in which carbon occurs in the investigated films are presented in Table 2. As can be seen, the combinations between carbon atoms in sp^2 hybridization are generally dominant, which proves the graphite-like structure of the carbon matrix. The differences in the concentration of sp^2 carbon in individual samples should be considered rather as a statistical distribution with an average value of 77 $\pm$ 3 at %, thus we do not see any correlation here with the activity of the methanation process, which does not mean, however, that the carbon matrix does not participate in this process through interaction with nickel speciation [55,59,60].
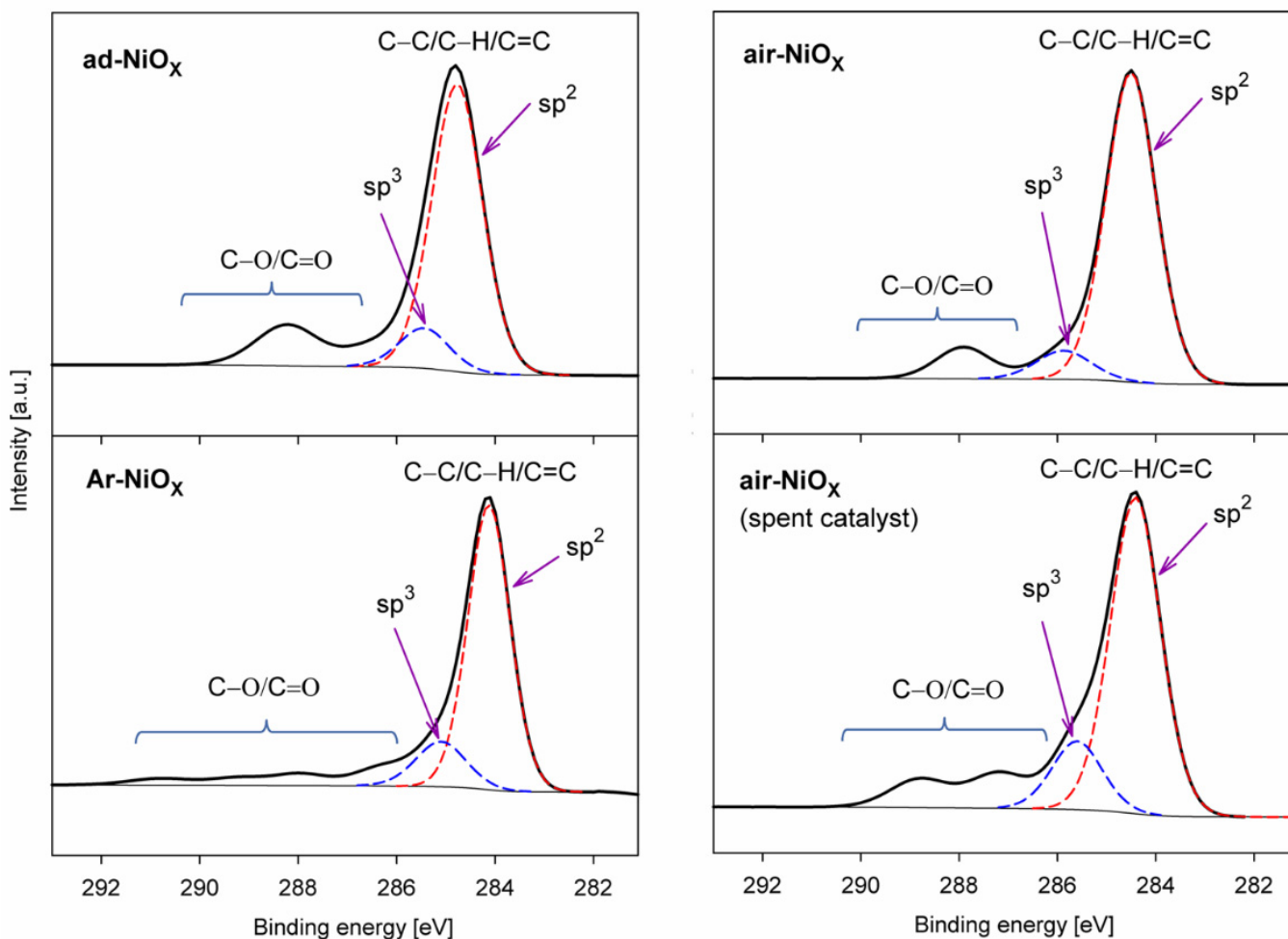
Figure 7. XPS C 1s spectra for all tested types of fresh plasma-deposited Ni-based films (ad-NiO$_X$, Ar-NiO$_X$, and air-NiO$_X$), as well as for the air-NiO$_X$ film after 37 h of the methanation process (spent catalyst).

3. Materials and Methods

The Ni-based films were produced by cold plasma deposition (PECVD) in a parallel-plate radio frequency (RF 13.56 MHz) plasma reactor working at low pressure. Details regarding the design of the reactor and the plasma deposition process are described elsewhere [3]. Tetracarbonyl nickel (Ni(CO)$_4$, Strem Chemicals, Inc., Newburyport, MA, USA),

used as a precursor, was directly introduced (without carrier gas) to the plasma chamber with a flow rate of 2.0 sccm. The glow discharge power and the pressure maintained in the chamber were 40 W and 4.5 Pa, respectively. The films were deposited for 30 min on kanthal steel supports (TermTech, Warsaw, Poland) in the form of knitted gauzes (mesh: 24×20 per inch, wire of 0.11 mm in diameter) for the catalytic tests and kanthal plates for SEM, XRD, and XPS measurements. Prior to the film deposition, the supports were calcined in air at 900 °C for 48 h. The aim of this process was to obtain a highly dispersed layer of alumina on the support to increase its surface area [3,5]. After deposition, part of the samples were thermally treated at 400 °C for 30 min in an argon atmosphere, and another part under the same conditions in an air atmosphere. Three types of films were further tested: films in the as-deposited state (ad-NiO_X), thermally treated in argon (Ar-NiO_X), and thermally treated in air (air-NiO_X).

Catalytic tests were carried out in a tubular quartz reactor (inner diameter of 2.3 cm, total length of 30 cm) under atmospheric pressure. The construction of the reactor used and the details of the measurement procedure are described in detail in our other work [39]. An inlet gas mixture for the CO_2 methanation process consisting of CO_2 (99.999%) and H_2 (99.7%) (Linde Gas, Cracow, Poland) was passed through the reactor with tested catalytic films (geometric area—38 cm^2) at a total flow rate of 25 sccm with a feed composition of H_2:CO_2 = 4:1. The exhaust gases were analyzed by using an on-line gas chromatograph (type 8610 C, SRI Instruments, Torrance, CA, USA) equipped with a thermal conductivity detector (TCD) and a HayeSep D column (Agilent, Santa Clara, CA, USA).

The surface topography of the films was studied by a scanning electron microscope Quanta 200 F (FEI, Hillsboro, OR, USA). All measurements were carried out under high vacuum conditions of approximately 10^{-5} Pa. The grain size distribution analysis was performed using the ImageJ software (version 1.53c, National Institutes of Health, Bethesda, MD, USA, 2020).

To determine the phase structure of the films, X-ray diffraction (XRD) was used. The diffractograms were obtained in the grazing incidence diffraction (GID) mode at 1.5 degrees. The patterns were measured by a PANalytical X'Pert Pro MD diffractometer with a Cu Kα X-ray source (1.5406 Å). The scanning range was 30–80° with a step of 0.02°.

The molecular structure of the surface of the tested films was investigated by X-ray photoelectron spectroscopy (XPS) using an AXIS Ultra spectrometer (Kratos Analytical Ltd., Manchester, UK) equipped with a monochromatic Al-Kα X-ray source (1486.6 eV). The power of the anode was set at 180 W, and the hemispherical electron energy analyzer was operated at pass energy of 20 eV for all high-resolution measurements. All measurements were carried out with a charge neutralizer. The component of the C 1s carbon line (which was assigned to sp^2 carbon), positioned at 284.4 eV, was used to calibrate the spectra. The background subtraction was performed with Shirley's function. The Kratos Vision 2 software (version 2.2.10, Kratos Analytical Ltd., Manchester, UK, 2012) was applied to the spectra deconvolution.

4. Conclusions

The PECVD method once again proved to be a useful tool for the production of thin-film catalysts, which are so important in the design of structured packings. As part of this study, nickel-based catalyst films were prepared using $Ni(CO)_4$ as a precursor, and then tested in the CO_2 methanation process. Contrary to the general opinion that the active phase in Ni-based catalysts in the CO_2 methanation process is metallic nickel, or possibly its composite with NiO, the performed studies showed a very good correlation between the catalytic activity of the films in this process, and the Ni^{3+} concentration in them, most likely in the form of Ni_2O_3. This finding opens a new chapter in research on the mechanism of CO_2 methanation over Ni-based nanocatalysts. Undoubtedly, further work is necessary on the role of Ni_2O_3 in this process and its possible cooperation with the NiO (Ni^{2+}) structure, as well as the graphite-like carbon matrix, which were identified in the studied films.

Data Availability Statement: The data is stored at the cloud (OneDrive) in the form of backup and is available on request from the corresponding author.

Conflicts of Interest: The authors declare no conflict of interest.

References

1. Tyczkowski, J. Cold Plasma produced catalytic materials. In *Plasma Science and Technology—Progress in Physical States and Chemical Reactions*; Mieno, T., Ed.; InTech Open: Vienna, Austria, 2016; pp. 53–93.
2. Wang, Z.; Zhang, Y.; Neyts, E.C.; Cao, X.; Zhang, X.; Jang, B.W.-L.; Liu, C. Catalyst preparation with plasmas: How does it work? *ACS Catal.* **2018**, *8*, 2093–2110. [CrossRef]
3. Tyczkowski, J.; Kierzkowska-Pawlak, H.; Kapica, R.; Balcerzak, J.; Sielski, J. Cold plasma—A promising tool for the production of thin-film nanocatalysts. *Catal. Today* **2019**, *337*, 44–54. [CrossRef]
4. Kołodziej, A.; Łojewska, J.; Tyczkowski, J.; Jodłowski, P.; Redzynia, W.; Iwaniszyn, M.; Zapotoczny, S.; Kuśtrowski, P. Coupled engineering and chemical approach to the design of a catalytic structured reactor for combustion of VOCs: Cobalt oxide catalyst on knitted wire gauzes. *Chem. Eng. J.* **2012**, *200–202*, 329–337. [CrossRef]
5. Kierzkowska-Pawlak, H.; Tyczkowski, J.; Balcerzak, J.; Tracz, P. Advances in plasma produced CoO_X-based nanocatalysts for CO_2 methanation. *Catal. Today* **2019**, *337*, 162–170. [CrossRef]
6. Kierzkowska-Pawlak, H.; Tracz, P.; Redzynia, W.; Tyczkowski, J. Plasma deposited novel nanocatalysts for CO_2 hydrogenation to methane. *J. CO_2 Util.* **2017**, *17*, 312–319. [CrossRef]
7. Centi, G.; Perathoner, S. Opportunities and prospects in the chemical recycling of carbon dioxide to fuels. *Catal. Today* **2009**, *148*, 191–205. [CrossRef]
8. Centi, G.; Quadrelli, E.A.; Perathoner, S. Catalysis for CO_2 conversion: A key technology for rapid introduction of renewable energy in the value chain of chemical industries. *Energy Environ. Sci.* **2013**, *6*, 1711. [CrossRef]
9. Bui, M.; Adjiman, C.S.; Bardow, A.; Anthony, E.J.; Boston, A.; Brown, S.; Fennell, P.S.; Fuss, S.; Galindo, A.; Hackett, L.A.; et al. Carbon capture and storage (CCS): The way forward. *Energy Environ. Sci.* **2018**, *11*, 1062–1176. [CrossRef]
10. Gac, W.; Zawadzki, W.; Słowik, G.; Sienkiewicz, A.; Kierys, A. Nickel catalysts supported on silica microspheres for CO_2 methanation. *Microporous Mesoporous Mater.* **2018**, *272*, 79–91. [CrossRef]
11. Branco, J.B.; Brito, P.E.; Ferreira, A.C. Methanation of CO_2 over nickel-lanthanide bimetallic oxides supported on silica. *Chem. Eng. J.* **2020**, *380*, 122465. [CrossRef]
12. Wang, W.; Duong-Viet, C.; Ba, H.; Baaziz, W.; Tuci, G.; Caporali, S.; Nguyen-Dinh, L.; Ersen, O.; Giambastiani, G.; Pham-Huu, C. Nickel nanoparticles decorated nitrogen-doped carbon nanotubes (Ni/N-CNT); a robust catalyst for the efficient and selective CO_2 methanation. *ACS Appl. Energy Mater.* **2019**, *2*, 1111–1120. [CrossRef]
13. Ridzuan, N.D.M.; Shaharun, M.S.; Lee, K.M.; Din, I.U.; Puspitasari, P. Influence of nickel loading on reduced graphene oxide-based nickel catalysts for the hydrogenation of carbon dioxide to methane. *Catalysts* **2020**, *10*, 471. [CrossRef]
14. Puga, A.V. On the nature of active phases and sites in CO and CO_2 hydrogenation catalysts. *Catal. Sci. Technol.* **2018**, *8*, 5681–5707. [CrossRef]
15. Tada, S.; Nagase, H.; Fujiwara, N.; Kikuchi, R. What are the best active sites for CO_2 methanation over Ni/CeO_2? *Energy Fuels* **2021**, *35*, 5241–5251. [CrossRef]
16. Lv, C.; Xu, L.; Chen, M.; Cui, Y.; Wen, X.; Li, Y.; Wu, C.E.; Yang, B.; Miao, Z.; Hu, X.; et al. Recent progresses in constructing the highly efficient Ni based catalysts with advanced low-temperature activity toward CO_2 methanation. *Front. Chem.* **2020**, *8*, 1–32. [CrossRef] [PubMed]
17. Pieta, I.S.; Lewalska-Graczyk, A.; Kowalik, P.; Antoniak-Jurak, K.; Krysa, M.; Sroka-Bartnicka, A.; Gajek, A.; Lisowski, W.; Mrdenovic, D.; Pieta, P.; et al. CO_2 hydrogenation to methane over Ni-catalysts: The effect of support and vanadia promoting. *Catalysts* **2021**, *11*, 433. [CrossRef]
18. Tada, S.; Shimizu, T.; Kameyama, H.; Haneda, T.; Kikuchi, R. Ni/CeO_2 catalysts with high CO_2 methanation activity and high CH_4 selectivity at low temperatures. *Int. J. Hydrog. Energy* **2012**, *37*, 5527–5531. [CrossRef]
19. Zhou, G.; Liu, H.; Cui, K.; Xie, H.; Jiao, Z.; Zhang, G.; Xiong, K.; Zheng, X. Methanation of carbon dioxide over Ni/CeO_2 catalysts: Effects of support CeO_2 structure. *Int. J. Hydrog. Energy* **2017**, *42*, 16108–16117. [CrossRef]
20. Zhang, Z.; Wei, T.; Chen, G.; Li, C.; Dong, D.; Wu, W.; Liu, Q.; Hu, X. Understanding correlation of the interaction between nickel and alumina with the catalytic behaviors in steam reforming and methanation. *Fuel* **2019**, *250*, 176–193. [CrossRef]

21. Taherian, Z.; Khataee, A.; Orooji, Y. Promoted nickel-based catalysts on modified mesoporous silica support: The role of yttria and magnesia on CO_2 methanation. *Microporous Mesoporous Mater.* **2020**, *306*, 110455. [CrossRef]

22. Shen, L.; Xu, J.; Zhu, M.; Han, Y.F. Essential role of the support for nickel-based CO_2 methanation catalysts. *ACS Catal.* **2020**, *10*, 14581–14591. [CrossRef]

23. Dias, Y.R.; Perez-Lopez, O.W. CO_2 conversion to methane using Ni/SiO_2 catalysts promoted by Fe, Co and Zn. *J. Environ. Chem. Eng.* **2021**, *9*, 104629. [CrossRef]

24. Ertl, G.; Knözinger, H.; Weitkamp, J. *Handbook of Heterogeneous Catalysis*; Wiley Company: Weinheim, Germany, 1997.

25. Garbarino, G.; Riani, P.; Magistri, L.; Busca, G. A study of the methanation of carbon dioxide on Ni/Al_2O_3 catalysts at atmospheric pressure. *Int. J. Hydrog. Energy* **2014**, *39*, 11557–11565. [CrossRef]

26. Yan, X.; Liu, Y.; Zhao, B.; Wang, Y.; Liu, C.J. Enhanced sulfur resistance of Ni/SiO_2 catalyst for methanation via the plasma decomposition of nickel precursor. *Phys. Chem. Chem. Phys.* **2013**, *15*, 12132–12138. [CrossRef] [PubMed]

27. Yan, X.; Liu, Y.; Zhao, B.; Wang, Z.; Wang, Y.; Liu, C.J. Methanation over Ni/SiO_2: Effect of the catalyst preparation methodologies. *Int. J. Hydrog. Energy* **2013**, *38*, 2283–2291. [CrossRef]

28. Mutz, B.; Gänzler, A.M.; Nachtegaal, M.; Müller, O.; Frahm, R.; Kleist, W.; Grunwaldt, J.D. Surface oxidation of supported Ni particles and its impact on the catalytic performance during dynamically operated methanation of CO_2. *Catalysts* **2017**, *7*, 279. [CrossRef]

29. Czekaj, I.; Loviat, F.; Raimondi, F.; Wambach, J.; Biollaz, S.; Wokaun, A. Characterization of surface processes at the Ni-based catalyst during the methanation of biomass-derived synthesis gas: X-ray photoelectron spectroscopy (XPS). *Appl. Catal. A Gen.* **2007**, *329*, 68–78. [CrossRef]

30. Zhao, Y.; Zhao, B.; Liu, J.; Chen, G.; Gao, R.; Yao, S.; Li, M.; Zhang, Q.; Gu, L.; Xie, J.; et al. Oxide-modified nickel photocatalysts for the production of hydrocarbons in visible light. *Angew. Chem. Int. Ed.* **2016**, *55*, 4215–4219. [CrossRef]

31. Bi, Q.; Huang, X.; Yin, G.; Chen, T.; Du, X.; Cai, J.; Xu, J.; Liu, Z.; Han, Y.; Huang, F. Cooperative catalysis of nickel and nickel oxide for efficient reduction of CO_2 to CH_4. *ChemCatChem* **2019**, *11*, 1295–1302. [CrossRef]

32. Huang, X.; Wang, P.; Zhang, Z.; Zhang, S.; Du, X.; Bi, Q.; Huang, F. Efficient conversion of CO_2 to methane using thin-layer SiO_X matrix anchored nickel catalysts. *New J. Chem.* **2019**, *43*, 13217–13224. [CrossRef]

33. Abu Bakar, W.A.W.; Othman, M.Y.; Ali, R.; Yong, C.K. Nickel oxide based supported catalysts for the in-situ reactions of methanation and desulfurization in the removal of sour gases from simulated natural gas. *Catal. Lett.* **2009**, *128*, 127–136. [CrossRef]

34. Abu Bakar, W.A.W.; Othman, M.Y.; Ali, R.; Yong, C.K.; Toemen, S. The investigation of active sites on nickel oxide based catalysts towards the in-situ reactions of methanation and desulfurization. *Mod. Appl. Sci.* **2009**, *3*, 35–43. [CrossRef]

35. Kreitz, B.; Arias, A.M.; Martin, J.; Weber, A.P.; Turek, T. Spray-dried Ni catalysts with tailored properties for CO_2 methanation. *Catalysts* **2020**, *10*, 1410. [CrossRef]

36. Bian, L.; Zhang, L.; Xia, R.; Li, Z. Enhanced low-temperature CO_2 methanation activity on plasma-prepared Ni-based catalyst. *J. Nat. Gas. Sci. Eng.* **2015**, *27*, 1189–1194. [CrossRef]

37. Zhao, B.; Yao, Y.; Shi, H.; Yang, F.; Jia, X.; Liu, P.; Ma, X. Preparation of Ni/SiO_2 catalyst via novel plasma-induced micro-combustion method. *Catal. Today* **2019**, *337*, 28–36. [CrossRef]

38. Jia, X.; Rui, N.; Zhang, X.; Hu, X.; Liu, C.J. Ni/ZrO_2 by dielectric barrier discharge plasma decomposition with improved activity and enhanced coke resistance for CO methanation. *Catal. Today* **2019**, *334*, 215–222. [CrossRef]

39. Kierzkowska-Pawlak, H.; Ryba, M.; Fronczak, M.; Kapica, R.; Sielski, J.; Sitarz, M.; Zając, P.; Łyszczarz, K.; Tyczkowski, J. Enhancing CO_2 conversion to CO over plasma-deposited composites based on mixed Co and Fe oxides. *Catalysts* **2021**, *11*, 883. [CrossRef]

40. Gong, J.; Wang, L.L.; Liu, Y.; Yang, J.H.; Zong, Z.G. Structural and magnetic properties of hcp and fcc Ni nanoparticles. *J. Alloys Compd.* **2008**, *457*, 6–9. [CrossRef]

41. García-Cerda, L.A.; Bernal-Ramos, K.M.; Montemayor, S.M.; Quevedo-López, M.A.; Betancourt-Galindo, R.; Bueno-Báques, D. Preparation of hcp and fcc Ni and Ni/NiO nanoparticles using a citric acid assisted Pechini-type method. *J. Nanomater.* **2011**, *2011*, 162495. [CrossRef]

42. Zhang, B.; Shang, X.; Jiang, Z.; Song, C.; Maiyalagan, T.; Jiang, Z.J. Atmospheric-pressure plasma jet-induced ultrafast construction of an ultrathin nonstoichiometric nickel oxide layer with mixed Ni^{3+}/Ni^{2+} ions and rich oxygen defects as an efficient electrocatalyst for oxygen evolution reaction. *ACS Appl. Energy Mater.* **2021**, *4*, 5059–5069. [CrossRef]

43. Richardson, J.T.; Scates, R.; Twigg, M.V. X-ray diffraction study of nickel oxide reduction by hydrogen. *Appl. Catal. A Gen.* **2003**, *246*, 137–150. [CrossRef]

44. Dey, S.; Bhattacharjee, S.; Chaudhuri, M.G.; Bose, R.S.; Halder, S.; Ghosh, C.K. Synthesis of pure nickel(III) oxide nanoparticles at room temperature for Cr(VI) ion removal. *RSC Adv.* **2015**, *5*, 54717–54726. [CrossRef]

45. Li, Y.; Wei, Z.; Ding, M.; Ma, L.; Zhu, X.; Liang, J. Synthesis and electrochemical properties of nickel oxide coated $ZnMn_2O_4$ nanocomposites. *J. Ceram. Soc. Jpn.* **2019**, *127*, 747–753. [CrossRef]

46. The Materials Project. *Materials Data on Ni_2O_3 (SG:63) by Materials Project*; Lawrence Berkeley National Laboratory: Berkeley, CA, USA, 2014. [CrossRef]

47. Olesen, S.E.; Andersson, K.J.; Damsgaard, C.D.; Chorkendorff, I. Deactivating carbon formation on a Ni/Al_2O_3 catalyst under methanation conditions. *J. Phys. Chem. C* **2017**, *121*, 15556–15564. [CrossRef]

48.	Bianchi, C.L.; Cattania, M.G.; Villa, P. XPS characterization of Ni and Mo oxides before and after "in situ" treatments. *Appl. Surf. Sci.* **1993**, *70–71*, 211–216. [CrossRef]

49.	Grosvenor, A.P.; Biesinger, M.C.; Smart, R.S.C.; McIntyre, N.S. New interpretations of XPS spectra of nickel metal and oxides. *Surf. Sci.* **2006**, *600*, 1771–1779. [CrossRef]

50.	Biesinger, M.C.; Payne, B.P.; Lau, L.W.M.; Gerson, A.; Smart, R.S.C. X-ray photoelectron spectroscopic chemical state quantification of mixed nickel metal, oxide and hydroxide systems. *Surf. Interface Anal.* **2009**, *41*, 324–332. [CrossRef]

51.	Chan, X.-H.; Jennings, J.R.; Hossain, A.; Yu, K.K.Z.; Wang, Q. Characteristics of p-NiO thin films prepared by spray pyrolysis and their application in CdS-sensitized photocathodes. *J. Electrochem. Soc.* **2011**, *158*, H733. [CrossRef]

52.	Chen, C.; Ogino, A.; Wang, X.; Nagatsu, M. Oxygen functionalization of multiwall carbon nanotubes by Ar/H_2O plasma treatment. *Diam. Relat. Mater.* **2011**, *20*, 153–156. [CrossRef]

53.	Feng, Y.; Yang, W.; Chen, S.; Chu, W. Cerium promoted nano nickel catalysts Ni-Ce/CNTs and Ni-Ce/Al_2O_3 for CO_2 methanation. *Integr. Ferroelectr.* **2014**, *151*, 116–125. [CrossRef]

54.	Yan, Y.; Dai, Y.; He, H.; Yu, Y.; Yang, Y. A novel W-doped Ni-Mg mixed oxide catalyst for CO_2 methanation. *Appl. Catal. B Environ.* **2016**, *196*, 108–116. [CrossRef]

55.	Swalus, C.; Jacquemin, M.; Poleunis, C.; Bertrand, P.; Ruiz, P. CO_2 methanation on Rh/γ-Al_2O_3 catalyst at low temperature: "In Situ" supply of hydrogen by Ni/activated carbon catalyst. *Appl. Catal. B Environ.* **2012**, *125*, 41–50. [CrossRef]

56.	Veerakumar, P.; Thanasekaran, P.; Subburaj, T.; Lin, K.-C. A Metal-free carbon-based catalyst: An overview and directions for future research. *C* **2018**, *4*, 54. [CrossRef]

57.	Gardner, S.D.; Singamsetty, C.S.K.; Booth, G.L.; He, G.-R.; Pittman, C.U. Surface characterization of carbon fibers using angle-resolved XPS and ISS. *Carbon* **1995**, *33*, 587–595. [CrossRef]

58.	Lesiak, B.; Kövér, L.; Tóth, J.; Zemek, J.; Jiricek, P.; Kromka, A.; Rangam, N. C sp^2/sp^3 hybridisations in carbon nanomaterials—XPS and (X)AES study. *Appl. Surf. Sci.* **2018**, *452*, 223–231. [CrossRef]

59.	Fidalgo, B.; Zubizarreta, L.; Bermúdez, J.M.; Arenillas, A.; Menéndez, J.A. Synthesis of carbon-supported nickel catalysts for the dry reforming of CH_4. *Fuel Process. Technol.* **2010**, *91*, 765–769. [CrossRef]

60.	Liu, S.; Yan, Z.; Zhang, Y.; Wang, R.; Luo, S.-Z.; Jing, F.; Chu, W. Carbon nanotubes supported nickel as the highly efficient catalyst for hydrogen production through glycerol steam reforming. *ACS Sustain. Chem. Eng.* **2018**, *6*, 14403–14413. [CrossRef]